


# Intrinsic temperature increase drives lipid metabolism towards ferroptosis evasion and chemotherapy resistance in pancreatic cancer

Received: 12 April 2023

Accepted: 26 September 2024

Published online: 02 October 2024

 Check for updates

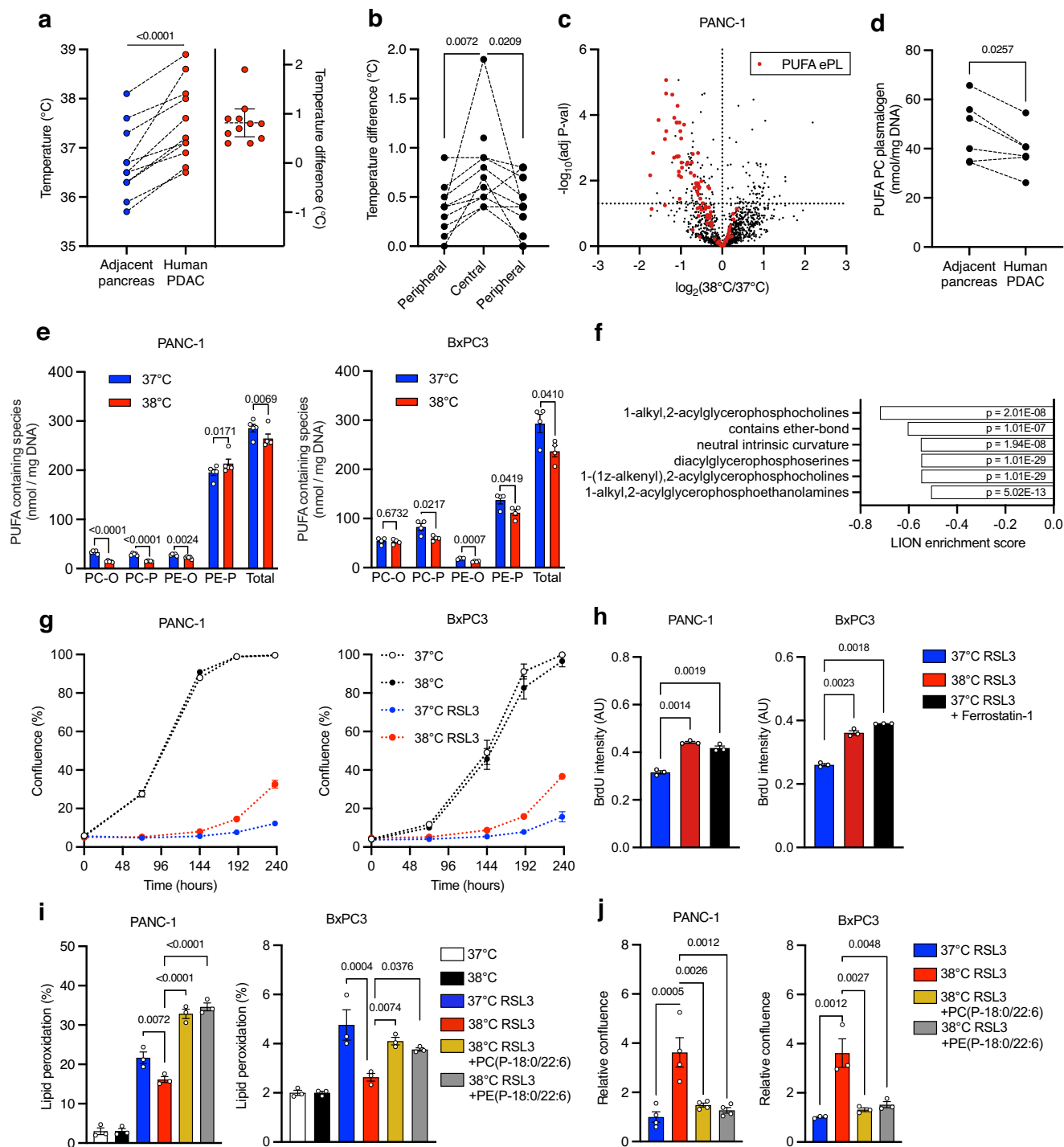
Vincent de Laat<sup>1</sup>, Halit Topal<sup>2</sup>, Xander Spotbeen<sup>1</sup>, Ali Talebi<sup>1</sup>, Jonas Dehairs<sup>1</sup>, Jakub Idkowiak<sup>1</sup>, Frank Vanderhoydonc<sup>1</sup>, Tessa Ostyn<sup>3</sup>, Peihua Zhao<sup>4</sup>, Maarten Jacquemyn<sup>5</sup>, Michele Wölk<sup>6</sup>, Anna Sablina<sup>4</sup>, Koen Augustyns<sup>7</sup>, Tom Vanden Berghe<sup>8,9</sup>, Tania Roskams<sup>3</sup>, Dirk Daelemans<sup>5</sup>, Maria Fedorova<sup>6</sup>, Baki Topal<sup>1,2</sup> & Johannes V. Swinnen<sup>1</sup> ✉

A spontaneously occurring temperature increase in solid tumors has been reported sporadically, but is largely overlooked in terms of cancer biology. Here we show that temperature is increased in tumors of patients with pancreatic ductal adenocarcinoma (PDAC) and explore how this could affect therapy response. By mimicking this observation in PDAC cell lines, we demonstrate that through adaptive changes in lipid metabolism, the temperature increase found in human PDAC confers protection to lipid peroxidation and contributes to gemcitabine resistance. Consistent with the recently uncovered role of p38 MAPK in ferroptotic cell death, we find that the reduction in lipid peroxidation potential following adaptation to tumoral temperature allows for p38 MAPK inhibition, conferring chemoresistance. As an increase in tumoral temperature is observed in several other tumor types, our findings warrant taking tumoral temperature into account in subsequent studies related to ferroptosis and therapy resistance. More broadly, our findings indicate that tumoral temperature affects cancer biology.

The development and progression of tumors unavoidably evokes changes in the tumor microenvironment. Cancer cells have to adapt to these changes in order to survive and thrive<sup>1</sup>. Hypoxia, acidosis, and nutrient deprivation are commonly studied examples of such changes. In contrast, altered temperature in solid tumors has been reported sporadically

but is largely overlooked in terms of cancer biology. A spontaneously occurring increase in tumoral temperature has been reported in case studies of human breast, lung and melanoma tumors<sup>2–4</sup>. This phenomenon is suspected to arise from increased metabolic heat generation and reduced blood flow when compared to healthy surrounding tissue<sup>5</sup>. Here

<sup>1</sup>Laboratory of Lipid Metabolism and Cancer, KU Leuven and Leuven Cancer Institute (LKI), Leuven, Belgium. <sup>2</sup>Abdominal Surgical Oncology, University Hospitals Leuven, KU Leuven and Leuven Cancer Institute (LKI), Leuven, Belgium. <sup>3</sup>Department of Pathology, University Hospitals Leuven, KU Leuven and Leuven Cancer Institute (LKI), Leuven, Belgium. <sup>4</sup>Laboratory for Mechanisms of Cell Transformation, VIB-KU Leuven Center for Cancer Biology, Leuven, Belgium. <sup>5</sup>Molecular Genetics and Therapeutics in Virology and Oncology, Rega Institute for Medical Research, KU Leuven Department of Microbiology and Immunology, Leuven, Belgium. <sup>6</sup>Center of Membrane Biochemistry and Lipid Research, Faculty of Medicine Carl Gustav Carus of TU Dresden, Dresden, Germany. <sup>7</sup>Department of Pharmaceutical Sciences, Laboratory of Medicinal Chemistry, University of Antwerp, Antwerp, Belgium. <sup>8</sup>Department of Biomedical Molecular Biology, VIB-UGent Center for Inflammation Research, Ghent, Belgium. <sup>9</sup>Department of Biomedical Sciences, University of Antwerp, Antwerp, Belgium. ✉e-mail: [j.swinnen@kuleuven.be](mailto:j.swinnen@kuleuven.be)



we show that human PDAC tumors invariably show an increase in tumoral temperature. We demonstrate that this modest increase in temperature evokes changes in ether lipids with poly-unsaturated fatty acids, which are particularly prone to lipid peroxidation. We further provide evidence that through deactivation of the p38 MAPK pathway, this adaptive change to temperature confers resistance to lipid peroxidation-mediated cell death, and contributes to resistance to gemcitabine, a standard chemotherapeutic treatment approach for PDAC.

## Results

### PDAC tumoral temperature is increased and drives ferroptosis evasion

To determine potential changes in temperature in PDAC tumors, we assessed the temperature of PDAC tumors and adjacent healthy

pancreatic tissue of 11 PDAC patients during standard laparoscopic surgery using a fiberoptic temperature probe. In all patients tested, we found increased temperature in PDAC tissue (Fig. 1a). Consistent with a mathematical model of temperature distribution in solid tumors<sup>5</sup>, we observed that temperature was most increased in the tumor center (Fig. 1b, Supplementary Data 1).

As cells are known to adapt to altered temperature by a homeoviscous mechanism involving changes in cellular lipid metabolism<sup>6</sup>, we analyzed the lipidome of PDAC cell lines PANC-1 and BxPC3 upon culture at increased temperature. For this, cells were cultured at 37 °C or 38 °C in designated and calibrated incubators. Lipidomics analysis revealed extensive alterations in the cellular lipidome (Fig. 1c, Supplementary Fig. 1a, Supplementary Data 2). Most notably, ether phospholipids (ePL) were downregulated in PDAC cells cultured at 38 °C

**Fig. 1 | PDAC tumoral temperature is increased and drives ferroptosis evasion.**

**a** Maximum temperature values in paired measurements of human PDAC and adjacent pancreas ( $n = 11$  patients). Paired two-sided Student's  $t$ -test. **b** Intratumoral temperature difference compared to adjacent pancreas ( $n = 11$  patients). Mixed-effects analysis with Dunnett's multiple comparisons test. **c** Volcano plot of the lipidomic analysis of PANC-1 cells upon culturing at 38 °C compared to 37 °C for 10 days ( $n = 5$  different wells in a single experiment, one representative experiment of 3 independent experiments is shown). Two-tailed Student's  $t$ -tests with Benjamini–Hochberg's multiple comparisons test. **d** PUFA PC plasmalogen content in available tissue from human PDAC and adjacent pancreas ( $n = 6$  patients). Paired two-sided Student's  $t$ -test. **e** Total abundance of PUFA containing ether lipid species (PC-O: 1-alkyl,2-acylphosphatidylcholine; PC-P: 1-alkenyl,2-acylphosphatidylcholine; PE-O: 1-alkyl,2-acylphosphatidylethanolamine; PE-P: 1-alkenyl,2-acylphosphatidylethanolamine) in PANC-1 ( $n = 5$  different wells, one representative experiment of 3 independent experiments is shown) or BxPC3 ( $n = 4$  different wells, one representative experiment of 2 independent experiments is shown) cells cultured at 37 °C or 38 °C for 10 days. Unpaired two-sided Student's  $t$ -test. **f** Downregulated

lipid ontology terms upon culturing PANC-1 cells ( $n = 5$  different wells) at 38 °C compared to 37 °C, as calculated by Lipid Ontology (LION) enrichment analysis web application. **g** Time-course confluence of PANC-1 or BxPC3 cells treated with RSL3, cultured at 37 °C or 38 °C ( $n = 3$  different wells, one representative experiment of 3 independent experiments is shown). **h** Proliferation as measured by BrdU incorporation of PANC-1 or BxPC3 cells treated with RSL3 for 10 days, cultured at 37 °C or 38 °C ( $n = 3$  different wells). One-way ANOVA with Šidák's multiple comparisons test. **i** Lipid peroxidation of PANC-1 cells or BxPC3 cells ( $n = 3$  different wells, one representative experiment of 2 independent experiments is shown) upon culturing at 38 °C for 10 days and treated with RSL3 or PUFA ePLs, normalized to control. One-way ANOVA with Šidák's multiple comparisons test. **j** Relative confluence of PANC-1 ( $n = 4$  different wells, one representative experiment of 2 independent experiments is shown) or BxPC3 cells ( $n = 3$  different wells, one representative experiment of 2 independent experiments is shown) upon culturing at 38 °C for 10 days and treated with RSL3 or PUFA ePLs, normalized to control. One-way ANOVA with Šidák's multiple comparisons test. Error bars represent s.e.m. from mean. Source data are provided as a Source Data file.

(Fig. 1c–f). Specifically, phosphatidylcholine plasmalogen (PC-P) species containing a poly-unsaturated fatty acid (PUFA) were decreased in PDAC cell lines upon culture at 38 °C (Fig. 1e). Consistent with these in vitro findings, we found decreased PUFA PC plasmalogen content in human PDAC compared to adjacent pancreas (Fig. 1d).

Importantly, PUFA ePL species are markedly prone to lipid peroxidation<sup>7</sup>. Moreover, cancer cells are able to adaptively downregulate PUFA ePLs as part of an antioxidant mechanism, driving resistance to ferroptosis, a lipid peroxidation-dependent form of cell death<sup>7,8</sup>. Analysis of PDAC cells cultured at 38 °C revealed a decrease in lipid peroxidation potential and reduced sensitivity to the ferroptosis-inducing compound RSL3 (Fig. 1g–i, Supplementary Fig. 1b). Supplementation of PUFA ePLs (PC-P-18:0-22:6) and PE(P-18:0-22:6)) restored RSL3-induced lipid peroxidation and concomitant sensitivity to RSL3 (Fig. 1i, j). In contrast to therapeutic hyperthermia temperature (43 °C), culturing PDAC cells at 38 °C did not affect cell growth (Supplementary Fig. 2), and subsequent lipidomic adaptations were not associated with alterations in membrane fluidity (Supplementary Fig. 3). Taken together, these findings indicate that the adaptive changes in lipid metabolism -upon temperature increase as found in human PDAC- do not reflect homeoviscous adaptation but rather allow PDAC cells to evade ferroptotic cell death.

**Ferroptosis evasion drives resistance to gemcitabine**

Ferroptosis induction was recently shown to extend survival of a genetically engineered mouse model of PDAC<sup>9</sup>. To further probe the clinical implications of ferroptosis in human PDAC, we evaluated the association between ferroptotic gene expression markers and survival of patients with PDAC from The Cancer Genome Atlas (TCGA). We found that reduced expression of ferroptosis suppressor genes is associated with increased survival (Fig. 2a). Given that ferroptosis is highly negatively regulated and that ferroptotic drivers are highly degenerate and promiscuous<sup>10</sup>, this finding indicates that ferroptotic cell death contributes to improved outcome for patients with PDAC. Based on our earlier findings in other tumor types that therapy resistance is associated with lipidomic alterations and concomitant sensitivity to lipid peroxidation<sup>11,12</sup>, we next examined whether a lipid peroxidation-mediated form of cell death is involved in the response to gemcitabine. This nucleoside analog is widely used as chemotherapy to treat pancreatic cancer<sup>13</sup> and has multiple mechanisms of action, many of which converge on the induction of apoptotic cell death<sup>14,15</sup>. Interestingly, resistance to gemcitabine can be targeted by combination treatments that sensitize PDAC cells to ferroptosis<sup>16–18</sup>, but whether gemcitabine itself induces ferroptosis has not been established<sup>19</sup>. To investigate how gemcitabine induces PDAC cell death, we tracked gemcitabine-induced apoptosis and lipid peroxidation over time. We found that gemcitabine initially induced

apoptosis, and subsequently induced lipid peroxidation-mediated cell death, as evidenced by increased lipid-ROS staining (Fig. 2b, c, Supplementary Fig. 4a, b), altered expression of ferroptosis markers (Fig. 2d, Supplementary Fig. 4c), appearance of a ferroptosis-like morphology (Fig. 2e), and accumulation of oxidized phospholipids (Fig. 2f) upon treatment with gemcitabine. To assess the contribution of evasion of a specific cell death type to gemcitabine resistance, we supplemented gemcitabine-treated PANC-1 and BxPC3 PDAC cells with the apoptosis inhibitor ZVAD, the ferroptosis inhibitor Ferrostatin-1, PD146176, an inhibitor of lipoxygenase-catalyzed lipid hydroperoxidation, and the necroptosis inhibitor Nec-1s. Our findings demonstrate that inhibiting lipid peroxidation, but not apoptosis or necroptosis, is sufficient to restore growth under gemcitabine treatment (Fig. 2g, Supplementary Fig. 4d, g). DFO, an iron chelator proved toxic during the time-course of our experiments (Supplementary Fig. 4e) hampering us to provide formal proof of the involvement of iron in the induction of cell death. Nevertheless, these results indicate that evasion of lipid-peroxidation-mediated cell death allows for resistance to gemcitabine in vitro.

Next, we found that the increased temperature of human PDAC tumors is not recapitulated by mouse PDAC models (Supplementary Fig. 5a–e), plausibly due to their unique features of thermal physiology<sup>20</sup>. Moreover, hypothermic murine PDAC temperature attenuated murine PDAC cell growth in vitro (Supplementary Fig. 5f), and human PDAC temperature-induced adaptations in PUFA-ePL abundance and ferroptosis resistance were also not recapitulated by murine PDAC cells (Supplementary Fig. 5g, h). Nonetheless, we found that gemcitabine also induced lipid peroxidation in PANC-1 xenografts in vivo (Fig. 2h). Additional treatment with UAMC-3203, a lead candidate ferroptosis inhibitor<sup>21,22</sup>, attenuated gemcitabine-induced lipid peroxidation (Fig. 2h) and allowed for gemcitabine resistance in vivo (Fig. 2i, j). Conversely, supplementation of PUFA ePL increased lipid peroxidation (Fig. 2h) and sensitized PANC-1 xenograft-bearing mice to gemcitabine (Fig. 2i, k). These results indicate that modulation of lipid peroxidation alters response to gemcitabine. Taken together, these findings support a causal role for ferroptosis evasion in gemcitabine resistance.

**PDAC temperature increase confers gemcitabine resistance**

We next wanted to evaluate if tumoral temperature alone is sufficient to drive gemcitabine resistance. Culturing PDAC cells at 38 °C indeed allowed for restoration of growth under gemcitabine treatment (Fig. 3a, b, Supplementary Fig. 6a–c, Supplementary Movie 1). To further elucidate the impact of different temperature variations, we also investigated additional temperature conditions beyond the previously examined range. Of note, our expanded analysis revealed that resistance to gemcitabine is influenced by a spectrum of temperature variations rather than a single point (Supplementary Fig. 6d, e).

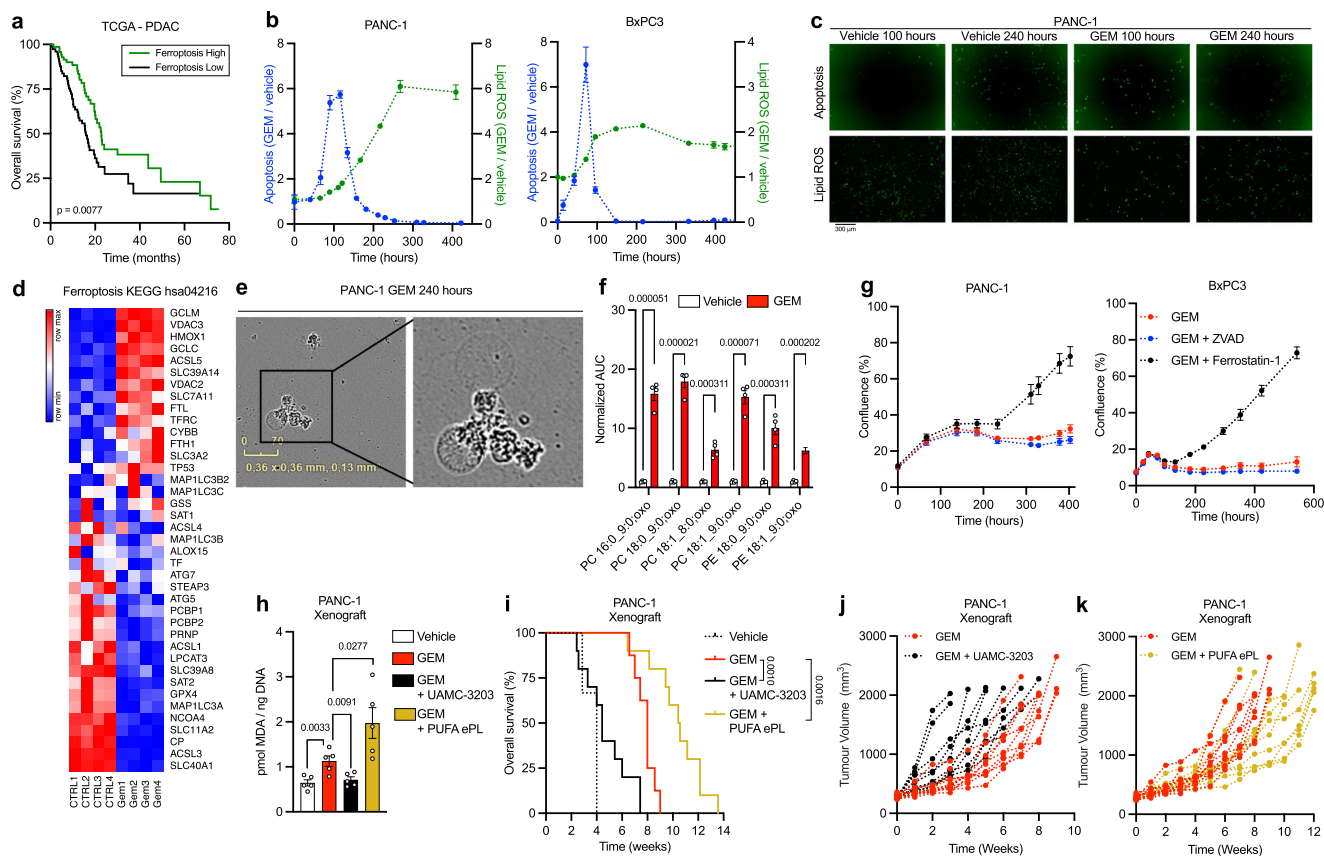


**Fig. 2 | Gemcitabine induces ferroptosis and ferroptosis evasion confers gemcitabine resistance.** **a** Overall survival of patients with PDAC with either high ( $n = 75$  patients, Ferroptosis Low) or low ( $n = 75$  patients, Ferroptosis High) expression of ferroptosis suppressor genes as determined by gene-expression signature (gene list provided in Supplementary Data 3). Log-rank (Mantel–Cox) test. **b** Relative apoptosis and lipid peroxidation of PANC-1 cells ( $n = 3$  different wells;  $n = 4$  different wells, respectively, one representative experiment of 2 independent experiments is shown) or BxPC3 cells ( $n = 6$  different wells;  $n = 5$  different wells) treated with gemcitabine (GEM) compared to vehicle. **c** Representative image of gemcitabine-induced apoptosis and lipid ROS after 100 h and 240 h in PANC-1 cells. **d** Expression of ferroptosis-related genes as measured by RNA-Seq in BxPC3 cells treated for 240 h with vehicle or gemcitabine ( $n = 4$  different wells). **e** Representative phase contrast image showing PANC-1 cells treated with gemcitabine undergoing cell death. **f** Oxidized lipid species in PANC-1 cells treated for 240 h with vehicle or gemcitabine ( $n = 4$  different wells). Unpaired two-sided Student's *t*-test with Holm–Šidák's multiple comparisons test. **g** Time-course

confluence of PANC-1 ( $n = 6$  different wells, one representative experiment of 3 independent experiments is shown) or BxPC3 ( $n = 8$ ;  $n = 4$ ;  $n = 2$  different wells, respectively, one representative experiment of 3 independent experiments is shown) cells treated with GEM, supplemented with ZVAD or Ferrostatin-1. **h** MDA abundance in harvested PANC-1 xenografts ( $n = 5$  mice) after one week of treatment with vehicle or gemcitabine (GEM), supplemented with UAMC-3203 or PUFA ePLs. One-way ANOVA with Šidák's multiple comparisons test. **i** Survival of PANC-1 xenograft bearing NMRInu/nu mice treated with vehicle ( $n = 3$  mice) or GEM ( $n = 8$  mice), supplemented with the ferroptosis inhibitor UAMC-3203 ( $n = 10$  mice) or PUFA ePLs ( $n = 10$  mice). Log-rank (Mantel–Cox) test. **j** Tumor volumes of individual PANC-1 xenograft bearing NMRInu/nu mice ( $n = 10$  mice) following treatment with gemcitabine (GEM), supplemented with UAMC-3203. **k** Tumor volumes of individual PANC-1 xenograft bearing NMRInu/nu nude mice following treatment with gemcitabine (GEM,  $n = 10$  mice) supplemented with PUFA ePLs ( $n = 11$  mice). Error bars represent s.e.m. from mean, but are not depicted when they are shorter than the symbol size. Source data are provided as a Source Data file.

Next, we found that temperature-induced resistance to gemcitabine was associated with a reduction in lipid peroxidation, and was phenocopied by supplementation of Ferrostatin-1 (Fig. 3c, d). Conversely, supplementation of PUFA ePLs normalized sensitivity to gemcitabine, an effect that could be prevented by additional supplementation of Ferrostatin-1 (Fig. 3e). These findings demonstrate that temperature increase as found in human PDAC is sufficient to allow for resistance to gemcitabine, through metabolic adaptation towards reduced lipid peroxidation potential.

### Lipidomic adaptations to temperature increase allow for p38 inhibition towards chemoresistance

Recent studies have demonstrated a mediating role for p38 MAPK activation in ferroptotic cell death downstream of lipid peroxidation<sup>23,24</sup>. Indeed, direct p38 MAPK inhibition or genetic knockout attenuated RSL3-induced cell death (Fig. 4a–c). In line with our finding that a low ferroptosis signature correlates with poor

survival (Fig. 2a), we found that p38 MAPK deactivation is associated with decreased survival of patients with PDAC (Fig. 4d). Moreover, we found that p38 MAPK activation was specific to PDAC cells in situ (Fig. 4e), and that p38 MAPK deactivation correlates with a low ferroptosis signature in clinical PDAC samples (Fig. 4f), confirming a clinical correlation between ferroptosis and p38 MAPK. Consistent with our finding that gemcitabine induces lipid peroxidation (Figs. 2b, c and 3c), we found that gemcitabine affects the expression of p38 MAPK pathway markers (Fig. 4g, Supplementary Fig. 7a) and induces p38 MAPK activation (Fig. 4h). Moreover, consistent with our finding that culturing cells at 38 °C prevents gemcitabine-induced lipid peroxidation (Fig. 3c), gemcitabine-induced p38 MAPK activation was prevented by culturing PDAC cells at 38 °C or by Ferrostatin-1 supplementation (Fig. 4h, Supplementary Fig. 7b, c). These findings indicate that the observed temperature-induced resistance to gemcitabine depends on p38 MAPK inhibition, and more broadly suggest that p38 MAPK inhibition contributes to resistance to gemcitabine in patients with PDAC.

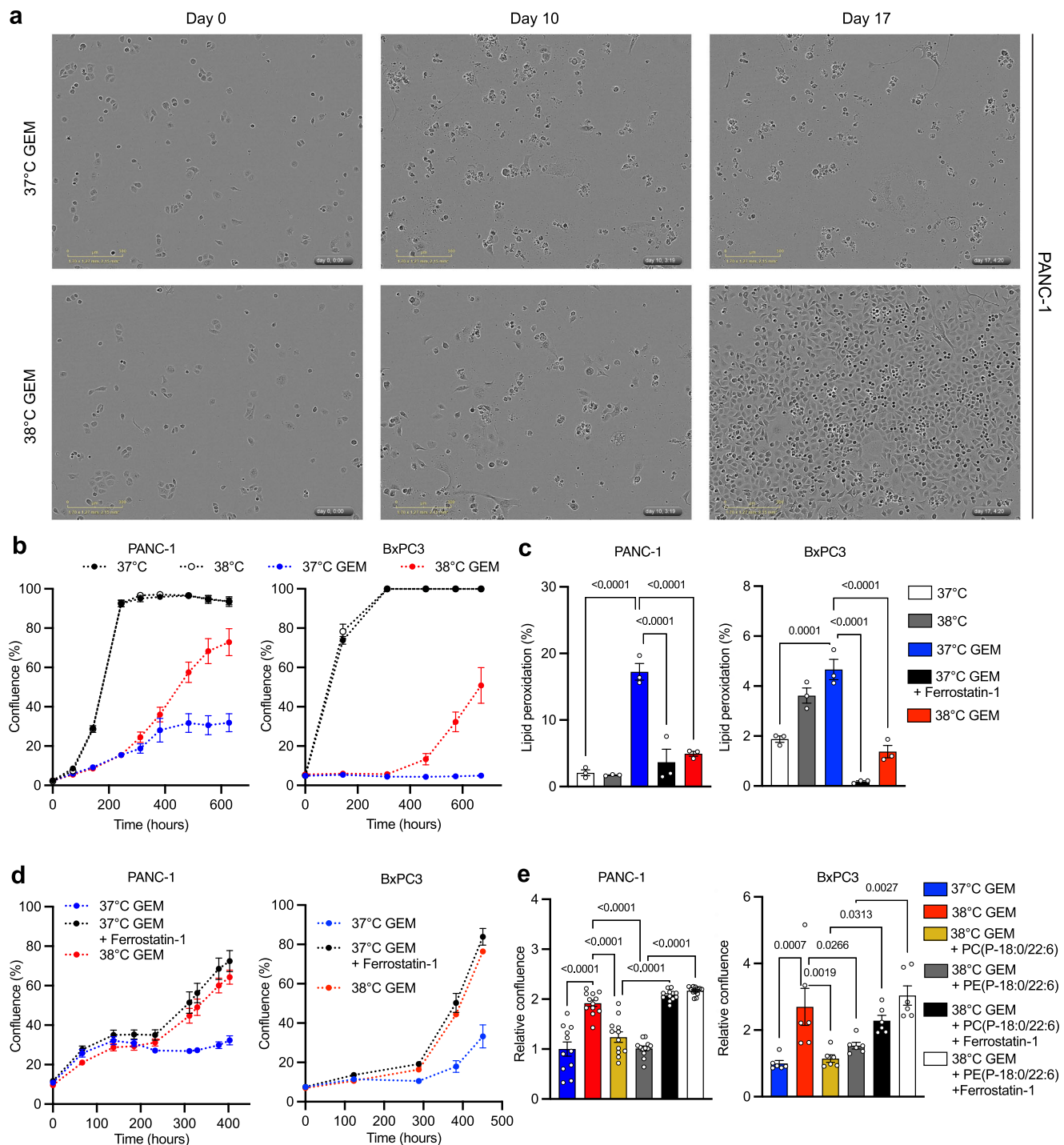
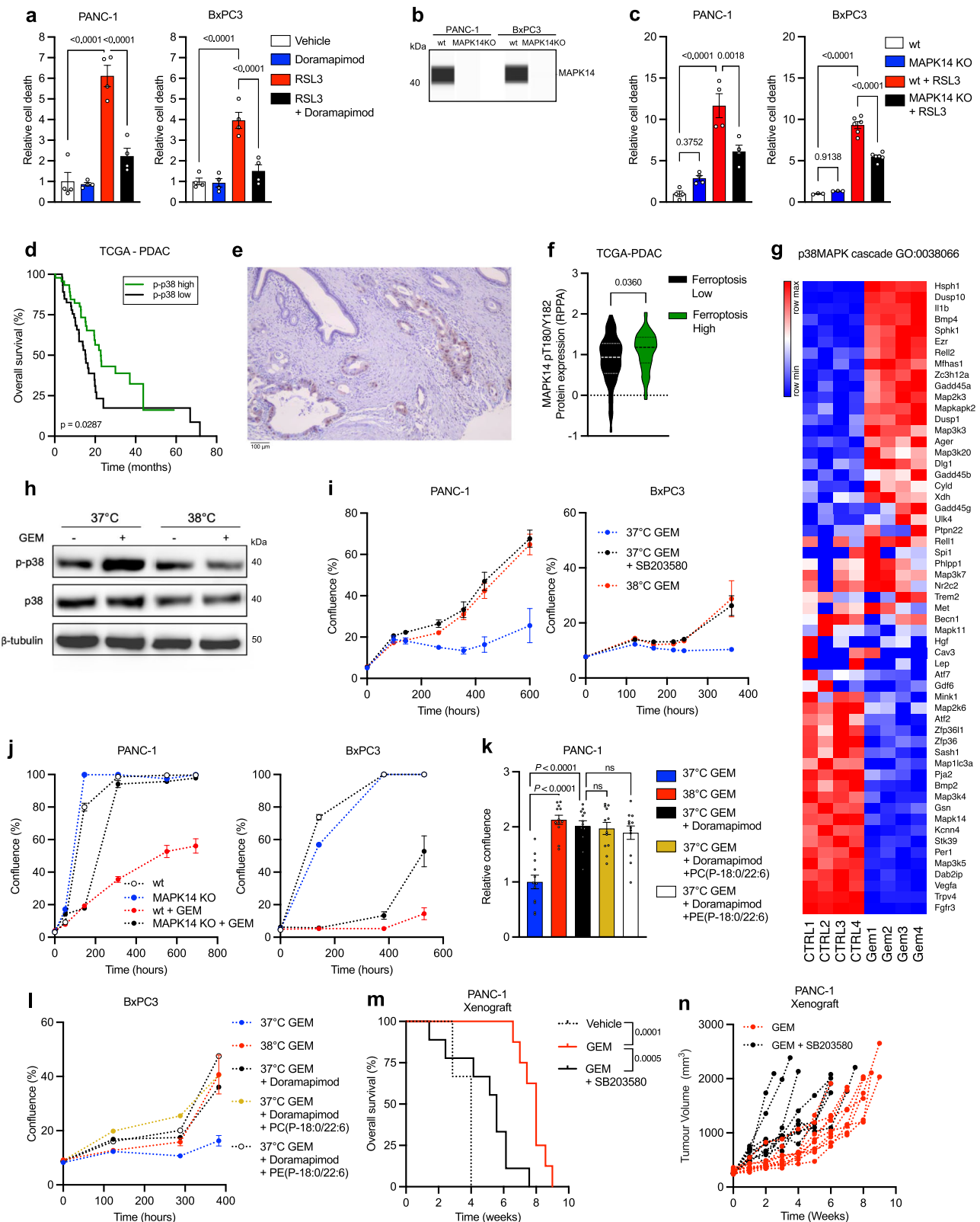


**Fig. 3 | Lipidomic adaptations to increased temperature drive gemcitabine resistance.** **a** Representative image of confluence at 0, 10 and 17 days of PANC-1 cells treated with gemcitabine (GEM), cultured at 37 °C or 38 °C. **b** Time-course confluence of PANC-1 ( $n = 4$ ) or BxPC3 ( $n = 12$ ;  $n = 6$  different wells, respectively, one representative experiment of 5 independent experiments is shown) cells treated with vehicle or GEM, cultured at 37 °C or 38 °C. **c** Lipid peroxidation of PANC-1 or BxPC3 cells treated with GEM, supplemented with Ferrostatin-1 or cultured at 38 °C for 10 days ( $n = 3$  different wells, one representative experiment of 2 independent experiments is shown). One-way ANOVA with Šidák's multiple comparisons test.

**d** Time-course confluence of PANC-1 or BxPC3 cells treated with GEM and Ferrostatin-1, cultured at 37 °C or 38 °C ( $n = 6$  different wells, one representative experiment of 3 independent experiments is shown). **e** Relative confluence of PANC-1 ( $n = 12$  different wells, one representative experiment of 2 independent experiments is shown) or BxPC3 ( $n = 6$  different wells, one representative experiment of 2 independent experiments is shown) cells upon culturing at 38 °C for 400 h and treated with GEM, PUFA ePLs and Ferrostatin-1, normalized to control. One-way ANOVA with Šidák's multiple comparisons test. Error bars represent s.e.m. from mean. Source data are provided as a Source Data file.

To investigate if p38 MAPK inhibition is sufficient to drive resistance to gemcitabine, we pharmacologically or genetically attenuated p38 MAPK and observed gemcitabine resistance in PDAC cells, phenocopying temperature-induced resistance to gemcitabine

(Fig. 4i–l). Notably, this effect could not be rescued by supplementation of PUFA ePLs (Fig. 4k, l), and direct p38 MAPK inhibition did not significantly affect PUFA ePL abundance (Supplementary Fig. 7d), corroborating earlier findings that p38 MAPK functions



downstream of lipid peroxidation<sup>23,24</sup>. Finally, we confirmed that non-toxic pharmacological inhibition of p38 MAPK drives resistance to gemcitabine in vivo (Fig. 4m, n, Supplementary Fig. 7e). Collectively, these results indicate that p38 MAPK inhibition acts downstream of temperature-induced adaptations in lipid metabolism, and demonstrate that p38 MAPK inhibition confers resistance to gemcitabine treatment in vivo.

## Discussion

Historically, the considered role of temperature in cancer biology and therapy response has been limited to fever, hyperthermia therapy and cold exposure, overlooking the native temperature of solid tumors<sup>25,26</sup>. PDAC is one of the most lethal solid tumors, in part through the complexity of its tumor microenvironment<sup>27</sup>. It is highly hypovascular<sup>28</sup> and has a rewired cellular metabolism<sup>29</sup>, which both

**Fig. 4 | p38 deactivation confers gemcitabine resistance downstream of temperature-induced adaptations in lipid metabolism.** **a** Cell death of PANC-1 or BxPC3 cells treated with RSL3 and Doramapimod for 24 h ( $n = 4$  different wells, one representative experiment of 2 independent experiments is shown). One-way ANOVA with Šidák's multiple comparisons test. **b** p-p38 expression in wild-type or MAPK14 KO PANC-1 and BxPC3 cells. **c** Cell death of wild-type or MAPK14 KO PANC-1 ( $n = 4$  different wells, one representative experiment of 2 independent experiments is shown) and BxPC3 ( $n = 3$ ;  $n = 6$  different wells, respectively) cells treated with vehicle or RSL3 for 24 h. One-way ANOVA with Šidák's multiple comparisons test. **d** Overall survival of patients with PDAC with either high ( $n = 47$  patients) or low ( $n = 48$  patients) p-p38 expression. Log-rank (Mantel–Cox) test. **e** Representative image of IHC staining for p-p38 in human PDAC (**f**) p38 activation status in patients with PDAC with either high ( $n = 55$  patients, Ferroptosis Low) or low ( $n = 53$  patients, Ferroptosis High) expression of ferroptosis suppressor genes. Unpaired two-sided Student's *t*-test. **g** Expression of p38 MAPK-related genes as measured by RNA-Seq in BxPC3 cells treated for 240 h with vehicle or gemcitabine ( $n = 4$  different wells). **h** Protein expression of p-p38 and p38 in PANC-1 cells treated with vehicle or GEM, cultured at 37 °C or 38 °C for 10 days. **i** Time-course confluence of PANC-1 ( $n = 4$  different wells, one representative experiment of 3

independent experiments is shown) or BxPC3 ( $n = 6$ ;  $n = 3$ ;  $n = 6$  different wells, respectively, one representative experiment of 3 independent experiments is shown) cells treated with GEM and supplemented with SB203580 or cultured at 38 °C. **j** Time-course confluence of wild-type or MAPK14 KO PANC-1 ( $n = 6$  different wells, one representative experiment of 2 independent experiments is shown) or BxPC3 ( $n = 6$ ;  $n = 12$  different wells, respectively, one representative experiment of 2 independent experiments is shown) cells treated with vehicle or GEM. **k** Relative confluence of PANC-1 cells treated with GEM and supplemented with Doramapimod and ePLs or cultured at 38 °C for 400 h ( $n = 12$  different wells, one representative experiment of 2 independent experiments is shown). One-way ANOVA with Šidák's multiple comparisons test. **l** Time-course confluence of BxPC3 cells treated with GEM and supplemented with Doramapimod and ePLs or cultured at 38 °C ( $n = 6$  different wells, one representative experiment of 2 independent experiments is shown). **m** Survival of PANC-1 xenograft bearing NMRInu/nu mice treated with vehicle ( $n = 3$  mice) or GEM ( $n = 8$  mice), supplemented with the p38 inhibitor SB203580 ( $n = 9$  mice). Log-rank (Mantel–Cox) test. **n** Tumor volumes of individual PANC-1 xenograft bearing NMRInu/nu mice following treatment with gemcitabine (GEM,  $n = 10$  mice) supplemented with SB203580 ( $n = 10$  mice). Error bars represent s.e.m. from mean. Source data are provided as a Source Data file.

are potential drivers of increased tumoral temperature<sup>5</sup>. Here, we unveil increased temperature as an inherent element of the human pancreatic tumor microenvironment. Of note, while our study successfully obtained temperature readings in patients with PDAC, potential uncertainties related to general anesthesia-induced hypothermia and depth of tumor location merit careful consideration. We therefore caution against direct inter-patient temperature comparisons.

We provide evidence that the modest temperature increase in human PDAC tumors stresses cancer cells sufficiently to trigger a previously discovered antioxidant mechanism<sup>7</sup>. By demonstrating that gemcitabine induces lipid peroxidation-mediated cell death and that ferroptosis inhibitors attenuate response to gemcitabine, we offer a new paradigm in the fundamental understanding of gemcitabine as well as its clinical use. Moreover, we highlight the importance of taking into account ferroptosis-modulating effects of investigational agents combined with ferroptosis-inducing chemotherapies. For example, as p38 MAPK inhibitors are known to inhibit ferroptotic cell death<sup>23,24</sup>, our findings offer a potential explanation for the lack of clinical significance that was found in a recent trial that evaluated the efficacy of addition of the p38 MAPK inhibitor ralimetinib to carboplatin and gemcitabine treatment in ovarian cancer<sup>30</sup>.

The role of lipid peroxidation in ferroptosis has been well-documented, with the accumulation of lipid peroxides being involved in disrupting membrane integrity, propagation of ROS, and the generation of degradation products that crosslink to DNA and proteins<sup>8,10</sup>. With its established role in stress response pathways, the activation of p38 in response to lipid peroxidation indicates an additional regulatory mechanism in the ferroptotic cell death process. Our findings add to previous studies that suggest a mediating role for p38 downstream of lipid peroxidation<sup>23,24</sup>, although further research is needed to delineate the exact molecular mechanisms by which p38 contributes to the ferroptotic process relative to the established and contextual roles of lipid peroxides.

Collectively, our findings uncover an unexplored link between the native temperature of human PDAC tumors, lipid peroxidation-mediated cell death, p38 MAPK and therapy response. Our finding that murine PDAC models are natively hypothermic highlights a novel critical shortcoming of mouse models in studying key aspects of cancer biology. As it is plausible that also other cell types are affected by the observed temperature increase in human tumors, it will be interesting to explore the effects of tumoral temperature in the context of other therapeutic modalities involving ferroptosis, such as immunotherapy.

## Methods

### Thermometry and collection of clinical samples

Patients provided written informed consent, and the procedure was approved by the UZ Leuven Medical Ethical Committee (S63521) and was carried out in accordance with the principles of the Declaration of Helsinki.

Temperature measurements in human patients were performed during laparoscopic pancreatic surgery under general anesthesia. The pancreatic tumor was surgically approached and localized with an intra-operative ultrasound device (BK 5000, BK Medical Holding Company, Inc.). First, a biopsy of the tumor was obtained using a trucut biopsy needle of 14 gauge (1.63 mm) diameter (Vigeo srl, Mantua, Italy), under ultrasound guidance. The resulting channel was used to introduce, under ultrasound guidance, the fiberoptic temperature probe (T1C-02-PP20, Neoptix, Qualitrol Company, Canada). The fiberoptic temperature probe was connected to the monitor (NOMAD fiber optic thermometer, Neoptix, Qualitrol Company, Canada) and the temperature registered. Temperature in healthy pancreatic tissue was measured at a distance of the tumor, and tumoral temperature was measured to obtain 3 measurement points within the tumor. Tissue samples were collected for downstream lipidomic analysis.

### Cell culture

PANC-1, BxPC3 and HPAC cells were obtained from ATCC. KPC cells were kindly provided by M. Mazzone (KU Leuven-VIB). Cell lines were propagated in DMEM High Glucose (Sigma), supplemented with 10% FBS (Life Technologies) and 4 mM glutamine (ThermoFisher). Cell cultures were periodically tested for mycoplasma contamination using the MycoAlert Mycoplasma Detection Kit (Lonza) and confirmed to be mycoplasma free.

For compound treatments, media was supplemented with 30 nM Gemcitabine (MedChem Express), 150 nM RSL3 (Selleck Chemicals), 5  $\mu$ M Doramapimod (Sigma), 10  $\mu$ M SB203580 (MedChem Express), 10 ZVAD (Sigma), 20  $\mu$ M Ferostatin-1 (Sigma), 2  $\mu$ M PD146176 (MedChem Express), 20  $\mu$ M Nec-1S (MedChem Express), 12.5–100  $\mu$ M DFO (Sigma) or 20  $\mu$ M PC/PE(P-18:0/22:6) (Sigma). To explore the effect of tumoral temperature, cells were cultured as indicated at 34 °C, 36 °C, 37 °C, 38 °C, 39 °C, 40 °C, or 43 °C in designated, calibrated and humidified incubators (IComed 150, Memmert) with 5% CO<sub>2</sub>. Key experiments were repeated in an independent pair of incubators (C150, Binder).

### Genetic MAPK14 knockout

CRISPR/Cas9-mediated knockouts were generated in the PANC-1 and BxPC3 cell lines using four different guides selected from the

Human Brunello CRISPR knockout pooled library (TGATGAAATGACAGGCTACG, CACAAAAACGGGGTTACGTG, AAGTAACCGCAGTTCTCTGT, CAAGGCGAGTAATACCTGTC). Guide sequences were cloned into the pLentiCRISPRv2 plasmid (Addgene, 52961) according to the standard cloning protocol. For lentiviral particle production, HEK293T cells (received from prof. Jason Moffat, Donnelly Centre, University of Toronto, Canada) were plated in 20 mL supplemented DMEM in T75 (TPP) flasks at 45% confluency and incubated overnight. 24 h later, the cells were co-transfected using Turbofectin 8.0 (OriGene, TF81001) with the pLentiCRISPR plasmids and the lentiviral packaging plasmids pMD2.G and psPAX2 to generate lentiviral particles coated with the VSV-G protein. Twenty-four hours post transfection the medium was changed to DMEM supplemented with serum-free BSA growth media (DMEM + 1.1 g/100 mL BSA and 20 µg/mL gentamicin). The supernatants containing lentiviral particles were harvested 72 h after transfection and stored at -80 °C. Cells were transduced with lentiviruses expressing a pool of the 4 sgRNAs and then selected with puromycin for 3 days.

For Jess Simple Western analysis (ProteinSimple), cells were lysed in RIPA lysis buffer (Sigma-Aldrich) for 1 h at 4 °C. Whole cell lysates were cleared by centrifugation. Proteins were separated by size using the 12–230 kDa Jess Separation Module (SM-W004) and bound with the primary antibody against MAPK14 (Cell Signaling, catalog no. 8690, diluted 1:100). Each of the bound antibodies were detected using the anti-rabbit detection module (DM-001, Protein Simple). Protein separation and detection was performed according to the manufacturer's instructions by capillary electrophoresis, antibody binding and visualization of HRP conjugates. Next, the primary and secondary antibodies were removed using the Replex Module (RP001, ProteinSimple) to allow sequential total protein detection. Protein signals were visualized using Compass Simple Western software, v.6.1.0 (ProteinSimple).

### Cell growth

Cells were seeded in 96-well plates at a density of  $4 \times 10^3$  cells per well and treated with the indicated compounds on the second day. Time-course cell growth (confluency) curves were generated using an IncuCyte ZOOM system (Sartorius) based on phase contrast images. When depicted as relative confluency, confluency was normalized to control at designated time points. Proliferation was measured by the BrdU cell proliferation assay (QIA58; Sigma Aldrich), according to the manufacturer's instructions.

### Membrane fluidity

Cells were stained with di-4-ANEPPDHQ (Thermo Fisher Scientific), according to the manufacturer's instructions. Cells were assayed using a FACS Verse flow cytometer (BD Biosciences). Samples were normalized to unstained control and generalized polarization (GP) was calculated with the following formula:  $(\text{Mean(FITC)} - \text{Mean(PE)}) / (\text{Mean(FITC)} + \text{Mean(PE)})$ .

### Lipidomics

For lipid extraction an amount of cells or tissue containing 10 µg of DNA was homogenized in 700 µL of water with a handheld sonicator and was mixed with 800 µL HCl(1 M):CH<sub>3</sub>OH 1:8 (v/v), 900 µL CHCl<sub>3</sub>, 200 µg/mL of the antioxidant 2,6-di-tert-butyl-4-methylphenol (BHT; Sigma Aldrich) and 3 µL of SPLASH® LIPIDOMIX® Mass Spec Standard (#330707, Avanti Polar Lipids). After vortexing and centrifugation, the lower organic fraction was collected and evaporated using a Savant Speedvac spd111v (Thermo Fisher Scientific) at room temperature and the remaining lipid pellet was stored at -20 °C under argon.

Just before mass spectrometry analysis, lipid pellets were reconstituted in 100% ethanol. Lipid species were analyzed by liquid chromatography electrospray ionization tandem mass spectrometry

(LC-ESI/MS/MS) on a Nexera X2 UHPLC system (Shimadzu) coupled with hybrid triple quadrupole/linear ion trap mass spectrometer (6500 + QTRAP system; AB SCIEX). Chromatographic separation was performed on a XBridge amide column (150 mm × 4.6 mm, 3.5 µm; Waters) maintained at 35 °C using mobile phase A (1 mM ammonium acetate in water-acetonitrile 5:95 (v/v)) and mobile phase B (1 mM ammonium acetate in water-acetonitrile 50:50 (v/v)) in the following gradient: (0–6 min: 0% B → 6% B; 6–10 min: 6% B → 25% B; 10–11 min: 25% B → 98% B; 11–13 min: 98% B → 100% B; 13–19 min: 100% B; 19–24 min: 0% B) at a flow rate of 0.7 mL/min which was increased to 1.5 mL/min from 13 min onwards. SM, CE, CER, DCER, HCER, LCER were measured in positive ion mode with a precursor scan of 184.1, 369.4, 264.4, 266.4, 264.4 and 264.4 respectively. TAG, DAG and MAG were measured in positive ion mode with a neutral loss scan for one of the fatty acyl moieties. PC, LPC, PE, LPE, PG, PI and PS were measured in negative ion mode by fatty acyl fragment ions. Lipid quantification was performed by scheduled multiple reactions monitoring (MRM), the transitions being based on the neutral losses or the typical product ions as described above. The instrument parameters were as follows: Curtain Gas = 35 psi; Collision Gas = 8 a.u. (medium); IonSpray Voltage = 5500 V and -4500 V; Temperature = 550 °C; Ion Source Gas 1 = 50 psi; Ion Source Gas 2 = 60 psi; Declustering Potential = 60 V and -80 V; Entrance Potential = 10 V and -10 V; Collision Cell Exit Potential = 15 V and -15 V.

The following fatty acyl moieties were taken into account for the lipidomic analysis: 14:0, 14:1, 16:0, 16:1, 16:2, 18:0, 18:1, 18:2, 18:3, 20:0, 20:1, 20:2, 20:3, 20:4, 20:5, 22:0, 22:1, 22:2, 22:4, 22:5 and 22:6 except for TGs which considered: 16:0, 16:1, 18:0, 18:1, 18:2, 18:3, 20:3, 20:4, 20:5, 22:2, 22:3, 22:4, 22:5, 22:6.

Peak integration was performed with the MultiQuant™ software version 3.0.3. Lipid species signals were corrected for isotopic contributions (calculated with Python Molmass 2019.1.1) and were quantified based on internal standard signals and adheres to the guidelines of the Lipidomics Standards Initiative (LSI) (level 2 type quantification as defined by the LSI). Unpaired T-test *p*-values and FDR corrected *p*-values (using the Benjamini/Hochberg procedure) were calculated in Python StatsModels version 0.10.1. Pathway enrichment analysis of the lipidomics data was conducted using the Lipid Ontology (LION) enrichment analysis web application<sup>31</sup>.

### Oxylipidomics

The following chemicals were used for oxylipidomics analysis: (ULC/MS-CC/SFC grade, >99.97%), methanol (UHPLC-MS grade, >99.97%), isopropanol (ULC/MS-CC/SFC grade, >99.95%), formic acid (ULC/MS-CC/SFC grade, >99%), and water (ULC/MS-CC/SFC grade) were obtained from Biosolve B.V. (Valkenswaard, Netherlands). Ammonium formate (MS grade), and butylated hydroxytoluene (BHT) were purchased from Sigma Aldrich Chemie GmbH (Taufkirchen, Germany). SPLASH LIPIDOMIX mixture of internal standards (ISTD) were obtained from Avanti Polar Lipids Inc (Alabaster, USA).

For lipid extraction, after harvesting cells, the samples were stored at -80 °C until further processing. On the analysis day, the samples were thawed on ice for -1 h, vortexed shortly, centrifuged (10 min, 4 °C, 10,000 × g) and supernatant was discarded. All solvents used for the extraction were supplemented with 0.1 % (w/v) BHT and cooled on ice before use. All extraction steps were performed on ice or at 4 °C. Cell pellets were resuspended in 50 µL of water. The samples were spiked with 2 µL of SPLASH LIPIDOMIX ISTD and incubated on ice for 15 min. Lipids were extracted following Folch protocol<sup>32</sup>. Briefly, to each sample 375 µL of methanol and 750 µL of chloroform were added. Samples were vortex and incubated for 1 h at 4 °C (orbital shaker, 32 rpm). Phase separation was induced by adding 625 µL of water. Samples were hand-shaken, vortexed, incubated for another 10 min at 4 °C (orbital shaker, 32 rpm), centrifuged (10 min, 4 °C, 1000 × g), lower organic phase containing lipids was collected into new tubes and

dried under vacuum. Aqueous phases were kept at  $-20^{\circ}\text{C}$  for the BCA Protein Assay for sample amount normalization.

For LPPtiger 2.0 assisted in silico prediction of oxidized lipids, 30 most abundant PUFA-containing PC, PE, and PE P- lipids (Supplementary Data 4) were used for in silico oxidation including hydroperoxy, hydroxy, epoxy, and keto groups as well as truncated derivatives. In silico oxidation was performed at the level 1, with a maximum of 2 oxidation sites, one <oxo> and one <OOH> modifications. Inclusion lists for semi-targeted LC-MS/MS analysis were produced using the Inclusion List Generator module within LPPtiger 2.0<sup>33</sup> and included elemental compositions of predicted oxidized lipids considering preferential ionization adducts (formate adduct anions for oxPC).

For semi-targeted detection of oxidized lipids, lipid extracts were reconstituted in 50  $\mu\text{L}$  isopropanol. 10  $\mu\text{L}$  of each sample were mixed to prepare total quality control (tQC) and experimental groups-specific (gQC) samples. 2.5  $\mu\text{L}$  (for high abundant in proteins) or 5  $\mu\text{L}$  (for low abundant in proteins) of gQC samples were loaded on an Accucore reverse phase C30 column (2.1  $\times$  150 mm, 2.6  $\mu\text{m}$ , 150  $\text{\AA}$ ; Thermo Fisher Scientific) installed on a Vanquish Horizon UHPLC (Thermo Fisher Scientific) coupled online to Exploris 240 Hybrid Quadrupole Orbitrap mass spectrometers equipped with a H-ESI source (Thermo Fisher Scientific). Lipids were separated by gradient elution with solvent A (acetonitrile/water, 1:1, v/v) and B (isopropanol/acetonitrile/water, 85:10:5, v/v/v) both containing 5 mM  $\text{NH}_4\text{HCO}_2$  and 0.1% (v/v) formic acid. Separation was performed at  $50^{\circ}\text{C}$  with a flow rate of 0.3 mL/min using following gradient: 0–20 min–10–80% B, 20–24 min–80–95% B, 24–27 min–95–100%, 27–32 min 100% (isocratic), 32.0–32.1 100–10% B, following 8 min of column equilibration at 10%.

Mass spectra were acquired in both positive and negative ion modes with the following ESI source settings: spray voltage – static, negative ion spray voltage 2500 V, gas mode – static, sheath gas – 40 (arbitrary units), aux gas – 10 (arbitrary units), sweep gas – 1 (arbitrary units), ion transfer tube temperature –  $300^{\circ}\text{C}$ , vaporizer temperature  $370^{\circ}\text{C}$ , S-lens RF level – 35%. In all methods, easy-IC was set to Run-Start. Semi-targeted analysis for detection of in silico predicted oxidized lipids was performed using data-dependent acquisition (DDA) and LPPtiger 2 generated inclusion list (Supplementary Data 5). A survey scan resolution of 60,000 at  $m/z$  200, AGC set to standard, and maximum injection time set to auto was used for the scan range of  $m/z$  500 to 980 (from minute 0 to 22) in negative polarity. Data-dependent MS2 (triggering only  $m/z$  values from the inclusion list) were collected with a resolution of 15,000 at  $m/z$  200, AGC target  $1\text{e}5$ , maximum injection time of 200 ms, isolation window of 1.5  $m/z$ , number of microscans 2, and stepped normalized collision energies (nCE; 22, 32, 43%). Isotopes and charge states  $>1$  were excluded. A Dynamic Exclusion was triggered after 5 MS/MS events, with an exclusion duration of 6 s and mass tolerance of 5 ppm.

For LPPtiger 2.0 assisted identification of oxidized lipids, acquired semi-targeted data files were converted to mzML files and opened in the LPPtiger 2.0<sup>33</sup> software to facilitate the identification of oxidized lipid species. All oxidized lipids identified by LPPtiger 2.0 were additionally confirmed by manual inspection of the corresponding MS/MS spectra (in Xcalibur QualBrowser Version 4.2.47, Thermo Fisher Scientific) and retention times mapping. Identified lipids were used to generate inclusion list for targeted parallel reaction monitoring (PRM) analysis.

For targeted analysis of oxidized lipids in individual samples for relative quantification of oxidized lipids, LC-coupled product ion scan (PIS) method was implemented for relative quantification of identified most abundant oxidized lipid species in individual samples. Lipid extracts (10  $\mu\text{L}$ ) were separated by C30 RPLC as described above. Mass spectra were acquired in negative ion mode with the following H-ESI source settings: spray voltage – static, ion spray voltage 2500 V, gas mode – static, sheath gas – 40 (arbitrary units), aux gas – 10 (arbitrary units), sweep gas – 1 (arbitrary units), ion transfer tube temperature –  $300^{\circ}\text{C}$ , vaporizer temperature  $370^{\circ}\text{C}$ , S-lens RF level – 35%. For PIS,

target mass lists were used in retention time-scheduled manner (start/end, Supplementary Data 6). MS/MS spectra were acquired at the resolution of 1500 at  $m/z$  200, AGC target  $1\text{e}5$  counts, Maximum IT 200 ms, isolation window 1.5  $m/z$ , stepped nCE 22, 32, 43%.

For data processing, the transitions corresponding to the loss of *sn*-1 and *sn*-2 acyl chains of oxidized species were used for the relative quantification. A list of transitions with retention times was generated and loaded into the Skyline software<sup>34</sup> (v 23.1.0.255) along with the acquired data. The peak integration of transitions corresponding to the elimination of both fatty acyls was verified and adjusted manually and the areas were extracted, averaged, recalculated against the standard, and normalized to the total protein content (normalized AUC).

For BCA analysis, protein was precipitated on ice by 12% TCA (trichloroacetic acid), centrifuged for 20 min at 12,000 G. Supernatant was removed and pellet was resuspended in 0.1 N NaOH. To determine protein content the Pierce Bicinchoninic Acid (BCA) Protein Assay Kit (Thermo Fisher Scientific) was used following the manufacturer's instructions.

### Lipid peroxidation assay

For lipid peroxidation, cells were seeded in 6-well plates at a density of  $3 \times 10^5$  cells per well. On the second day, the cells were treated with the indicated compounds for 10 days. Lipid peroxidation was measured using BODIPY<sup>TM</sup> 581/591 C11 reagent (ThermoFisher), according to the manufacturer's instructions. Cells were assayed using a FACS Verse instrument (BD Biosciences) and lipid peroxidation was assessed as described previously<sup>35</sup>. Briefly, cells with a FITC/PE fluorescence ratio greater than 98% of the untreated cells are defined as lipid ROS positive. For time course lipid peroxidation experiments, cells were seeded in 96-well plates at a density of  $4 \times 10^3$  cells per well and treated with 5  $\mu\text{M}$  BODIPY<sup>TM</sup> 581/591 C11 on the second day. The IncuCyte ZOOM system (Sartorius) was used to quantify lipid peroxidation over time.

### Apoptosis

Cells were seeded in 96-well plates at a density of  $4 \times 10^3$  cells per well and treated with the indicated compounds on the second day. Apoptosis was measured using Invitrogen<sup>TM</sup> CellEvent<sup>TM</sup> Caspase-3/7 Green Detection Reagent (ThermoFisher), according to the manufacturer's instructions. The IncuCyte ZOOM system (Sartorius) was used to quantify apoptosis over time.

### Western blot

Western blotting was carried out on PDAC cell lines. Following ice-cold PBS washes, cells were collected in sample buffer (ThermoFisher) supplemented with DTT (Sigma), sonicated and boiled for 5 min. Equal amounts of protein were loaded onto precast gels (NuPAGE, ThermoFisher), transferred to nitrocellulose membranes, and incubated with antibodies against phospho-p38 MAPK (1/1000 dilution) (Cell Signaling, #4511) and p38 MAPK (1/1000 dilution) (Cell Signaling, #8690).

### Patient survival data

The survival and expression data of patients with pancreatic cancer were evaluated from the PDAC database of The Cancer Genome Atlas (TCGA-PAAD). Ferroptosis signature value was determined by single-sample gene set enrichment analysis (ssGSEA) (S Hänzelmann et al.<sup>36</sup>). The genes used for the ferroptosis signature (Supplementary Data 3) are from the FerrDb database<sup>37</sup>. Protein expression of MAPK14 (pPT180/Y182) was used to probe p38 phosphorylation status and patients were stratified into quartiles using the cBioPortal<sup>38</sup>.

### Gene expression

For gene expression, cells were seeded in 6-well plates at a density of  $3 \times 10^5$  cells per well. On the second day, the cells were treated with gemcitabine for 10 days. RNA was isolated using the PureLink<sup>TM</sup> RNA

Mini Kit (12183018A, Invitrogen). Libraries were constructed and bulk RNA-seq were performed by Novogene (UK).

### Immunohistochemistry

Manual DAB staining was performed on formalin-fixed paraffin embedded (FFPE) sections of human PDAC tumors cut at 5  $\mu$ m. After dewaxing, antigen epitope retrieval was performed using the EnVision FLEX Target Retrieval Solution High pH (ref K800421-2) in a PT link instrument (Agilent, ref PT20027). Endogenous peroxidase was blocked for 5 min using the Dako REAL Peroxidase-Blocking Solution (ref S202386-2). Slides were incubated with primary antibody to phospho-p38 MAPK (Thr180/Tyr182) (1:200; Cell Signaling, #4511), followed by a horseradish peroxidase (HRP)-labeled secondary antibody for 30 min each. 3,3'-Diaminobenzidine (DAB) chromogen was added for visualization of the staining (10 min) and slides were counterstained with hematoxylin, rehydrated and mounted. Images were captured using the Zeiss Axioscan.Z1 slide scanner.

### Animal experiments

All procedures involving animals were carried out in accordance with the guidelines of the IACUC and the Animal Care and Use Ethical Committee (KU Leuven, P036/2021). All animals were co-housed (3–5 animals/cage) in individually ventilated cages (Tecniplast Blue Line IVC system) with ad libitum access to drinking water and standard chow (Sniff® R/M-H, V1535-000, Sniff Spezialdiäten).

For murine tumoral temperature measurements,  $5 \times 10^5$  PANC-1 cells or  $1 \times 10^5$  KPC cells dissolved in PBS were injected subcutaneously or orthotopically into 6–8 week old female NMRInu/nu mice (Janvier) or C57BL/6j mice (Janvier), respectively. Orthotopic tumors were allowed to grow until palpable, subcutaneous tumors were allowed to grow up to sizes between 250 and 1000 mm<sup>3</sup> before temperature was measured.

To probe the effect of ferroptosis modulation and p38 inhibition on gemcitabine response,  $5 \times 10^5$  PANC-1 cells were injected subcutaneously into 6–8 week-old female NMRInu/nu mice (Janvier). Tumors were allowed to grow to 250 mm<sup>3</sup> before mice were allocated to treatment and control group by stratified randomization. Tumor bearing mice were either treated with vehicle, gemcitabine (UZ Leuven Hospitals, 50 mg/kg, twice weekly by intraperitoneal injection) UAMC-3203 (2% DMSO in saline, 6 mg/kg, daily by intraperitoneal injection), Doramapimod (AdooQ, 0.5% methylcellulose (Sigma), 50 mg/kg, twice weekly by oral gavage) or ether lipids (10  $\mu$ M PC(P-18:0/22:6) and 10  $\mu$ M PE(P-18:0/22:6) (Sigma) dissolved in water as described previously<sup>7</sup>, twice weekly by intratumoral injection). Tumor size was measured with a digital caliper (Fowler Sylvac) and mice were euthanized upon reaching humane endpoints (tumor size exceeding 2000 mm<sup>3</sup> or ulcerating tumors), after which tumors were collected and snap-frozen for further analysis.

Temperature measurements in mouse models were performed under general anesthesia, in subcutaneous or orthotopic models. Temperature was measured using a fiberoptic temperature probe (TIC-02-PP20, Neoptix, Qualitrol Company, Canada) connected to a monitor (NOMAD fiber optic thermometer, Neoptix, Qualitrol Company, Canada). Infrared images were taken with a camera (PI400 IR-camera, Optris - kindly provided by W. Saeys (KU Leuven)) for demonstrative purposes.

### Statistical analysis

The results were analyzed using GraphPad Prism v.9.1.2. Statistical data analysis was performed on  $n \geq 3$  replicates. Details on statistical tests and post-tests are presented in the figure legends.  $p$ -values of  $<0.05$  were considered to be statistically significant.

### Reporting summary

Further information on research design is available in the Nature Portfolio Reporting Summary linked to this article.

### Data availability

All data, including patient information and tumoral temperature data, lipidomics data, survival and expression data of patients with pancreatic cancer and the genes used for the ferroptosis signature, are available in the main text or the supplementary materials. The mass spectrometry data generated in this study have been deposited in the public MassIVE repository under accession code [MSV000095706](https://doi.org/10.1038/s41467-024-52978-z). The bulk RNA-seq data generated in this study have been deposited at the NCBI Gene Expression Omnibus (GEO) under accession number [GSE249302](https://doi.org/10.1038/s41467-024-52978-z). Source data are provided with this paper.

### References

- Hanahan, D. & Weinberg, R. A. Hallmarks of cancer: the next generation. *Cell* **144**, 646–674 (2011).
- Gautherie, M. Thermopathology of breast cancer: measurement and analysis of in vivo temperature and blood flow. *Ann. N. Y. Acad. Sci.* **335**, 383–415 (1980).
- Stefanadis, C. et al. Temperature differences are associated with malignancy on lung lesions: a clinical study. *BMC Cancer* **3**, 1 (2003).
- Shada, A. L. et al. Infrared thermography of cutaneous melanoma metastases. *J. Surg. Res.* **182**, e9–e14 (2013).
- Bousselham, A., Bouattane, O., Youssfi, M. & Raihani, A. Brain tumor temperature effect extraction from MRI imaging using bioheat equation. *Proc. Comput. Sci.* **127**, 336–343 (2018).
- Sinensky, M. Homeoviscous adaptation—a homeostatic process that regulates the viscosity of membrane lipids in *Escherichia coli*. *Proc. Natl Acad. Sci. USA* **71**, 522–525 (1974).
- Zou, Y. et al. Plasticity of ether lipids promotes ferroptosis susceptibility and evasion. *Nature* **585**, 603–608 (2020).
- Dixon, S. J. et al. Ferroptosis: an iron-dependent form of non-apoptotic cell death. *Cell* **149**, 1060–1072 (2012).
- Badgley, M. A. et al. Cysteine depletion induces pancreatic tumor ferroptosis in mice. *Science* **368**, 85–89 (2020).
- Hassannia, B., Vandenabeele, P. & Vanden Berghe, T. Targeting ferroptosis to iron out cancer. *Cancer Cell* **35**, 830–849 (2019).
- Rysman, E. et al. De novo lipogenesis protects cancer cells from free radicals and chemotherapeutics by promoting membrane lipid saturation. *Cancer Res.* **70**, 8117–8126 (2010).
- Talebi, A. et al. Sustained SREBP-1-dependent lipogenesis as a key mediator of resistance to BRAF-targeted therapy. *Nat. Commun.* **9**, 2500 (2018).
- Burris, H. A. et al. Improvements in survival and clinical benefit with gemcitabine as first-line therapy for patients with advanced pancreatic cancer: a randomized trial. *J. Clin. Oncol.* **15**, 2403–2413 (1997).
- Huang, P. & Plunkett, W. Induction of apoptosis by gemcitabine. *Semin. Oncol.* **22**, 19–25 (1995).
- Schniewind, B. et al. Resistance of pancreatic cancer to gemcitabine treatment is dependent on mitochondria-mediated apoptosis. *Int. J. Cancer* **109**, 182–188 (2004).
- Lister, A. et al. Nrf2 is overexpressed in pancreatic cancer: implications for cell proliferation and therapy. *Mol. Cancer* **10**, 37 (2011).
- Zhu, S. et al. HSPA5 regulates ferroptotic cell death in cancer cells. *Cancer Res.* **77**, 2064–2077 (2017).
- Ye, Z. et al. FBW7-NRA41-SCD1 axis synchronously regulates apoptosis and ferroptosis in pancreatic cancer cells. *Redox Biol.* **38**, 101807 (2021).
- Yang, J. et al. Ferroptosis: at the crossroad of gemcitabine resistance and tumorigenesis in pancreatic cancer. *Int. J. Mol. Sci.* **22**, 10944 (2021).
- Gordon, C. J. The mouse thermoregulatory system: its impact on translating biomedical data to humans. *Physiol. Behav.* **179**, 55–66 (2017).
- Devisscher, L. et al. Discovery of novel, drug-like ferroptosis inhibitors with in vivo efficacy. *J. Med. Chem.* **61**, 10126–10140 (2018).

22. Van Coillie, S. et al. Targeting ferroptosis protects against experimental (multi)organ dysfunction and death. *Nat. Commun.* **13**, 1046 (2022).
23. Hattori, K. et al. Cold stress-induced ferroptosis involves the ASK1-p38 pathway. *EMBO Rep.* **18**, 2067–2078 (2017).
24. Ye, F. et al. HMGB1 regulates erastin-induced ferroptosis via RAS-JNK/p38 signaling in HL-60/NRASQ61L cells. *Am. J. Cancer Res.* **9**, 730–739 (2019).
25. Repasky, E. A., Evans, S. S. & Dewhirst, M. W. Temperature matters! And why it should matter to tumor immunologists. *Cancer Immunol. Res.* **1**, 210–216 (2013).
26. Seki, T. et al. Brown-fat-mediated tumour suppression by cold-altered global metabolism. *Nature* **608**, 421–428 (2022).
27. Ho, W. J., Jaffee, E. M. & Zheng, L. The tumour microenvironment in pancreatic cancer - clinical challenges and opportunities. *Nat. Rev. Clin. Oncol.* **17**, 527–540 (2020).
28. Kahn, B. M. et al. The vascular landscape of human cancer. *J. Clin. Invest.* **131**, 136655 (2021).
29. Perera, R. M. & Bardeesy, N. Pancreatic cancer metabolism: breaking it down to build it back up. *Cancer Discov.* **5**, 1247–1261 (2015).
30. Vergote, I. et al. A randomized, double-blind, placebo-controlled phase 1b/2 study of ralimetinib, a p38 MAPK inhibitor, plus gemcitabine and carboplatin versus gemcitabine and carboplatin for women with recurrent platinum-sensitive ovarian cancer. *Gynecol. Oncol.* **156**, 23–31 (2020).
31. Molenaar, M. R. et al. LION/web: a web-based ontology enrichment tool for lipidomic data analysis. *Gigascience* **8**, giz061 (2019).
32. Folch, J., Lees, M. & Sloane Stanley, G. H. A simple method for the isolation and purification of total lipides from animal tissues. *J. Biol. Chem.* **226**, 497–509 (1957).
33. Criscuolo, A. et al. Analytical and computational workflow for in-depth analysis of oxidized complex lipids in blood plasma. *Nat. Commun.* **13**, 6547 (2022).
34. Adams, K. J. et al. Skyline for Small Molecules: A Unifying Software Package for Quantitative Metabolomics. *J. Proteome Res.* **19**, 1447–1458 (2020).
35. Zhang, H.-L. et al. PKC $\beta$ II phosphorylates ACSL4 to amplify lipid peroxidation to induce ferroptosis. *Nat. Cell Biol.* **24**, 88–98 (2022).
36. Hänzelmann, S., Castelo, R. & Guinney, J. GSEA: gene set variation analysis for microarray and RNA-seq data. *BMC Bioinformatics* **14**, 7 (2013).
37. Zhou, N. & Bao, J. FerrDb: a manually curated resource for regulators and markers of ferroptosis and ferroptosis-disease associations. *Database (Oxford)* **2020**, baaa021 (2020).
38. Cerami, E. et al. The cBio cancer genomics portal: an open platform for exploring multidimensional cancer genomics data. *Cancer Discov.* **2**, 401–404 (2012).

## Acknowledgements

We thank all patients that participated in this study. We thank Lotte Bral for cell line production. V.d.L. is a recipient of a PhD fellowship from the Research Foundation – Flanders (FWO) with support from Kom op Tegen Kanker, and received a research grant from the Rik en Nel Wouters donation. X.S. was supported by a PhD fellowship from the Research Foundation – Flanders (FWO). K.A. and T.V.B. are part of a consortium of excellence focusing on inflammation (INFLA-MED). This work was supported by a grant from the Belgian Foundation Against Cancer (2018-088 to J.V.S.). Work in the Fedorova lab is supported by “Sonderzuweisung zur Unterstützung profilbestimmender Struktureinheiten” by the SMWK to TUD, TG70 by Sächsische Aufbaubank and SMWK, the measure is co-financed with tax funds on the basis of the budget passed by the Saxon state parliament (to M.F.), Deutsche Forschungsgemeinschaft (FE 1236/5-1 to M.F.), and Bundesministerium für Bildung und Forschung (01EJ2205A, FERROPath to M.F.). This article is

based upon work from COST Action EpiLipidNET, CA19105, supported by COST (European Cooperation in Science and Technology).

## Author contributions

V.d.L.: Conceptualization, Acquisition of data, Analysis and interpretation of data, Isolation of clinical material, Development of methodology, Writing and revision of the manuscript, H.T.: Development of methodology, Acquisition of data. X.S.: Isolation of clinical material, Acquisition of data. A.T.: Development of methodology, Acquisition of data, Review of the manuscript. J.D.: Development of methodology, Acquisition of data, Analysis and interpretation of data. J.I.: Development of methodology, Acquisition of data, Analysis and interpretation of data. F.V.: Acquisition of data. T.O.: Isolation of clinical material. P.Z.: Analysis and interpretation of data. M.J.: Development of methodology, Acquisition of data. M.W.: Development of methodology, Acquisition of data, Analysis and interpretation of data. A.S.: Analysis and interpretation of data. K.A.: Compound synthesis and treatment optimization. T.V.B.: Compound synthesis and treatment optimization, T.R.: Isolation of clinical material. D.D.: Development of methodology. M.F.: Development of methodology, Acquisition of data, Analysis and interpretation of data. B.T.: Development of methodology, Acquisition of data. J.V.S.: Study supervision, Review of the manuscript, Acquisition of funding.

## Competing interests

T.V.B. and K.A. hold patents US9862678, WO2016075330, EP3218357, and WO2019154795 related to ferrostatin-1 analogs. The remaining authors declare no competing interests.

## Additional information

**Supplementary information** The online version contains supplementary material available at <https://doi.org/10.1038/s41467-024-52978-z>.

**Correspondence** and requests for materials should be addressed to Johannes V. Swinnen.

**Peer review information** *Nature Communications* thanks Robert Ivkov, Francisco X. Real, and the other, anonymous, reviewer(s) for their contribution to the peer review of this work. A peer review file is available.

**Reprints and permissions information** is available at <http://www.nature.com/reprints>

**Publisher's note** Springer Nature remains neutral with regard to jurisdictional claims in published maps and institutional affiliations.

**Open Access** This article is licensed under a Creative Commons Attribution-NonCommercial-NoDerivatives 4.0 International License, which permits any non-commercial use, sharing, distribution and reproduction in any medium or format, as long as you give appropriate credit to the original author(s) and the source, provide a link to the Creative Commons licence, and indicate if you modified the licensed material. You do not have permission under this licence to share adapted material derived from this article or parts of it. The images or other third party material in this article are included in the article's Creative Commons licence, unless indicated otherwise in a credit line to the material. If material is not included in the article's Creative Commons licence and your intended use is not permitted by statutory regulation or exceeds the permitted use, you will need to obtain permission directly from the copyright holder. To view a copy of this licence, visit <http://creativecommons.org/licenses/by-nc-nd/4.0/>.

© The Author(s) 2024